PCCP

Electrochemical, spectroscopic and SPM evidence for the controlled formation of self-assembled monolayers and organised multilayers of ferrocenyl alkyl thiols on Au(111)

A. S. Viana,[ab] L. M. Abrantes,[b] G. Jin,[c] S. Floate,[d] R. J. Nichols[d] and M. Kalaji*[a]

[a] *Department of Chemistry, University of Wales Bangor, Bangor, Gwynedd, UK LL57 2UW. E-mail: m.kalaji@bangor.ac.uk*
[b] *CECUL, Departamento de Química e Bioquímica, Faculdade de Ciências, Universidade de Lisboa, Campo Grande, 1700 Lisboa, Portugal*
[c] *Laboratory of Laser Research, Institute of Mechanics, Chinese Academy of Sciences, Beijing 100080, P.R. China*
[d] *Department of Chemistry, University of Liverpool, Crown Street, Liverpool, UK L69 7ZD*

Received 13th February 2001, Accepted 13th June 2001
First published as an Advance Article on the web 18th July 2001

Organised multilayers were formed from the controlled self-assembly of ferrocene alkyl thiols on Au(111) surfaces. The control was accomplished by increasing the concentration of the thiol solutions used for the assembly. Cyclic voltammetry, ellipsometry, scanning probe microscopy (STM and AFM) and *in situ* FTIR spectroscopy were used to probe the differences between mono- and multilayers of the same compounds. Electrochemical desorption studies confirmed that the multilayer structure is attached to the surface *via* one monolayer. The electrochemical behaviour of the multilayers indicated the presence of more than one controlling factor during the oxidation step, whereas the reduction was kinetically controlled which contrasts with the behaviour of monolayers, which exhibit kinetic control for the oxidation and reduction steps. Conventional and imaging ellipsometry confirmed that multilayers with well-defined increments in thickness could be produced. However, STM indicated that at the monolayer stage, the thiols used promote the mobility of Au atoms on the surface. It is very likely that the multilayer structure is held together through hydrogen bonding. To the best of out knowledge, this is the first example of a controlled one-step growth of multilayers of ferrocenyl alkyl thiols using self-assembly techniques.

Introduction

Self-assembled monolayers (SAMs) are prepared by the spontaneous adsorption of organic molecules from homogeneous solutions. Strategies for modifying electrode surfaces to control electrochemical reactivity *via* immobilised molecules have become highly developed, indicating great promise in the area of electronic and optical devices, chemical sensors, and models for the study of interfacial reactivity and fundamental charge transfer processes.[1–4]

Self-assembly deposition of alkyl thiols normally results in the formation of monolayers at the Au(111) surface. However, ensembles with thicknesses that were inconsistent with monolayer formation were also observed from the self-assembly of long chain alkyl thiols ($n > 10$).[5–7]

Practical applications based on self-assembled monolayers are well documented in the literature;[8–11] however, organised multilayers, with controlled thickness values, formed through self-assembly may also exhibit properties that are of considerable technological interest. These may include applications in corrosion prevention and lubrication, in addition to their use in sensors where the dynamic range may be increased compared to those based on monolayers.

There are currently no established procedures for the formation, in a one-step process, of such organised supramolecular structures even though the controlled formation of thick layers has been reported by a variety of authors;[1,12] such thick layers were always considered inconvenient and their formation and properties were not characterised.

In the present study short chain ferrocenyl alkyl thiols with a carbonyl functionality $(C_5H_5)Fe(C_5H_4)CO(CH_2)_nSH$ ($n = 2$, 4, 5 and 9) were assembled on single crystal gold (111) electrodes.

Redox centres, such as ferrocene, which are incorporated as terminal groups into SAMs, provide a probe for both the monolayer structure and kinetic parameters associated with the redox switching of the layers. Surface coverage of modified electrodes can be quantitatively assessed with good precision using standard electrochemical methods.[13–15]

The inclusion of the carbonyl group was to enable the monitoring of orientational changes using IR spectroscopy. Cyclic voltammetry, conventional *ex situ* ellipsometry, imaging ellipsometry and scanning probe microscopies (scanning tunnelling microscopy (STM) and atomic force microscopy (AFM)) were used to characterise the modified surfaces prepared under different adsorption conditions in order to evaluate the dependence of the resulting films on the deposition conditions.

The expected structural changes that accompany the redox switching of the organised layers were monitored using *in situ* FTIR spectroscopy and the data were compared with those previously reported for organised monolayers of the same monomers.

Experimental

Chemicals

The ferrocene derivatives $(C_5H_5)Fe(C_5H_4)CO(CH_2)_nSH$ [(FcC_n; where $n = 3$, 5, 6 and 10 and $Fc = (C_5H_5)Fe(C_5H_4)$]

DOI: 10.1039/b101435h

were all synthesised using available reagents. Here the synthesis of FcC_6 is described but the same scheme was used for the synthesis of all the compounds.[16] A solution of ferrocene (2.54 g, 0.0268 mol) in CH_2Cl_2 (50 ml) was mixed with a solution of 6-bromohexanoyl chloride (4 g, 0.0188 mol in 10 ml CH_2Cl_2) in a three-necked round-bottomed flask. A quiescent layer of Ar was kept over the mixture. Aluminium chloride (1.818 g, 0.0136 mol) was added to the mixture. The colour of the solution turned from orange to purple after the addition of the latter. The mixture was stirred for 4 h after which the reaction was quenched by the addition of hydrochloric acid (100 ml, 0.1 mol dm^{-3}). The aqueous layer was separated and washed twice with CH_2Cl_2 (50 ml aliquots). The organic layers were combined and dried over anhydrous $MgSO_4$. The solvent was removed using a rotary evaporator leaving behind a thick oil of crude 6-bromoalkanoylferrocene. This was then mixed with silica and ether, which was evaporated leaving behind a brown powder. The powder was then turned into slurry by mixing it with a small amount of petroleum ether (40/60). The pure product was separated through column chromatography, first by eluting with 5% ether/95% petroleum ether, followed by 10% ether/90% petroleum ether. The product was characterised by spectral comparison with authentic samples previously prepared; IR spectroscopy (ν(C=O), 1667 cm^{-1}; ν(C–H) ferrocene, 3109 cm^{-1}; ν(C–H) alkyl chain, 2963 cm^{-1}).

The bromide was then converted to the thiol. Thiourea (0.7 g, 0.009 mol) was dissolved in ethanol (30 ml) and the solution was refluxed. An ethanolic solution of 6-bromoalkanoylferrocene (4 g, 0.01 mol in 10 ml of ethanol) was added to the mixture which was further heated for 4 h after which NaOH (0.06 g in 10 ml H_2O) was added. The solution was allowed to cool to room temperature, and then acidified with dilute HCl. The organic layer was separated and washed with water. The aqueous layer was washed with ethyl acetate. The organic fractions were combined and the solvent was removed under reduced pressure. The thiol was then purified through a silica gel column using 95% petroleum ether (40/60) and 5% ethyl acetate.

^{1}H NMR: 1.40–1.59 (ms, 6H), 2.56 (m, 2H); 2.90 (m, 2H), 4.20 (s, 5H), 4.45 (t, 2H); 4.75 (t, 2H). The total overall yield was 51%.

The other compounds were synthesised in a similar fashion except that the length of the alkyl chain in the bromoalkanoyl chloride was varied.

For the electrochemical and SNIFTIR measurements perchloric acid (Aristar, BDH) was used as received. Ultra pure UV-treated water was obtained from an Elgastat UHQ II purification system. Absolute ethanol was used as received for the deposition of the SAMs.

Substrates

Gold slides (Metalhandel Schröer GmbH, Germany) were used for the electrochemical experiments, and were obtained by evaporating 200 nm Au on glass slides (Tempax AF 45) which had been previously coated with a Cr layer (2–4 nm). Prior to use, the gold slides (1.1 × 1.1 cm^2) were flame annealed in a Bunsen burner until the slide attained red heat several times. After cooling in air for a short period of time, the slide was quenched in water. This treatment produces a flat gold surface with strong Au(111) characteristics.[17] *In situ* FTIR measurements were performed using an Au single-crystal (111) electrode (Metal Crystals and Oxides, Ltd., Cambridge, England) that was polished to a mirror finish using alumina (down to 0.05 μm) followed by electropolishing in a solution of 95% ethanol : 5% HCl for a few minutes using a current density of approximately 0.33 A cm^{-2}. Finally, the electrodes were flame-annealed in a Bunsen flame and quenched in water.

Electrode modification

The gold substrate (single-crystal disc or gold-coated glass) was immersed in ethanolic or toluene solutions of varying concentrations of ferrocenylalkylthiols (1–3, 10 and 30–40 mmol dm^{-3}), for periods of 20 to 24 h. Deposition was performed in the dark under normal laboratory conditions (room temperature). After assembly, the electrodes were rinsed with copious amounts of absolute ethanol and water.

Electrochemistry

All glassware was cleaned using a 50 : 50 mixture of concentrated H_2SO_4 : HNO_3 followed by rinsing with purified water and cleaning in a steam bath. Cyclic voltammetry was performed using a DT2101 Hi-Tek potentiostat, a PPRI Hi-Tek waveform generator, and a Yokohama 3023 X–Y recorder. A one compartment Teflon cell, with an Au wire spiral counter electrode and a saturated calomel reference electrode (SCE) was used. The Au slide was clamped against an o-ring, which defined the geometric area (0.6 cm^2). The electrolyte solution ($HClO_4$, 1 mol dm^{-3}) was degassed for 15 min prior to the start of any measurement.

Ellipsometry

Ex situ ellipsometric results were obtained using a rotating analyser type SENTECH Ellipsometer (SENTECH Instruments GmbH, Berlin, Germany) fitted with a He–Ne laser (632.8 nm). The measurements were carried out at an angle of incidence of 70°. The gold electrodes were examined before and after immersion in the deposition solution. Imaging ellipsometry[18] was performed using an expanded light beam instead of the conventional narrow beam. Once the null conditions are fulfilled for the bare substrate, the thickness of any film on the surface is then proportional to the square root of the reflected light intensity. The source was a xenon lamp with a 632.8 nm interference filter and a collimating system to ensure a uniform intensity distribution over the beam area. The photomultiplier detector was replaced by a CCD video camera (752 × 582 pixels) and suitable optics allowing more than 4 × 10^5 surface areas on a 7 × 25 mm^2 sample surface to be concurrently measured. The video signal was digitised, captured and stored in a greyscale format.

Scanning probe microscopy

The STM imaging was performed with a PicoSPM system (Molecular Imaging Corporation) and a Nanoscope E controller (Digital Instruments Corporation). STM measurements were carried out in air at room temperature and in constant current mode. The STM tips were mechanically fabricated from Pt–Ir wire. Tapping mode or intermittent contact mode AFM images were obtained on a Nanoscope III scanning probe microscope (Digital Instruments). N-doped AFM sensors (Nanosensors) were used for the tapping mode AFM measurements (resonant frequency of 245–432 Hz).

Spectroelectrochemistry

Subtractively normalised interfacial Fourier transform infrared spectroscopy (SNIFTIRS) measurements were performed in a staircase mode using a fully evacuated FTIR spectrometer (Bruker IFS113v) fitted with a mercury cadmium telluride (MCT) photodetector, p-polariser and Ge/KBr beam splitter. The single-crystal electrode was assembled at the end of a Teflon holder, which allows flexibility, when the electrode is pushed against the infrared transparent silicon window. A Pt foil and a SCE were used as the counter and reference electrode, respectively. Fig. 1 shows a sketch of the spectroelectrochemical cell used in this work.

The difference spectra were obtained by subtracting two

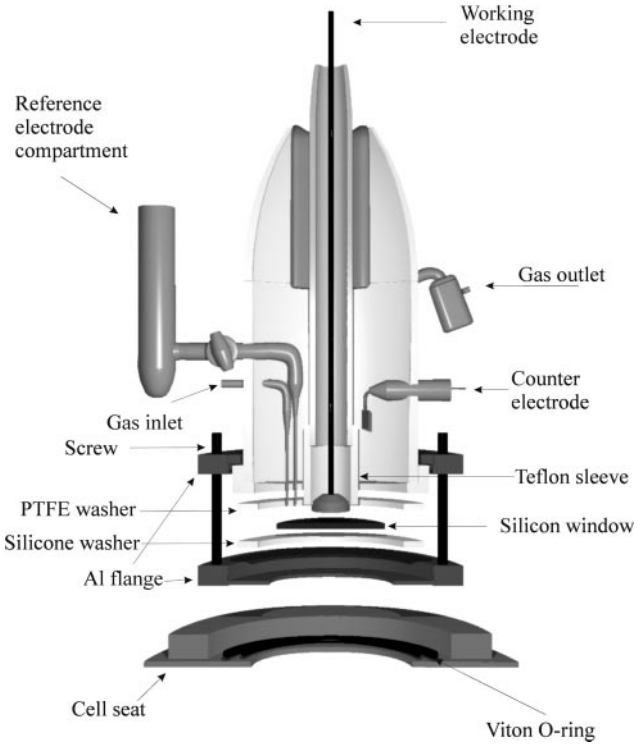

Fig. 1 A diagram showing the cell used for the SNIFTIR studies.

spectra (S2 − S1) collected at different potentials (E2 and E1, respectively) and dividing by the spectrum obtained at E1 (S1). The positive and negative bands in the normalised difference spectra indicate decreased and increased absorbances, respectively at E2. Throughout these studies 300 interferograms were collected at each potential. Since no logarithm was applied, the difference spectra are shown as reflectance units ($\Delta R/R$). The electrochemical control was accomplished using a potentiostat (Hi-Tek, DT2101) and waveform generator (Hi-Tek PPR1). All the experiments were performed using perchloric acid (0.5 mol dm^{-3}) in D_2O.

Results and discussion

Electrochemical studies

As expected, the redox behaviour of all the modified electrodes reported in this work, is dominated by the ferrocene/ferricenium couple. The stability, order and packing of the films were assessed by cyclic voltammetry. Fig. 2 shows typical cyclic voltammograms obtained for gold-coated glass electrodes modified with FcC_6 and FcC_{10} from dilute solutions (a) and (c) and concentrated solutions (b) and (d), respectively.

The electrochemical parameters obtained from the voltammograms (Γ, surface coverage; $E_{1/2}$, half-wave potential; ΔE_p, redox peak separation; and $\Delta E_{p,1/2}$, total width at half-height) are summarised in Table 1. The values for the surface coverage, which were calculated from the oxidation charge, take into account the roughness factor (1.2) of the gold-coated slides, which has been calculated from iodine chemisorption measurements.

It is clear from the data and shape of the voltammograms that adsorption of the same compound under different conditions produces films with distinct electrochemical behaviour. The surface coverage (based on the area of ferrocene redox peaks) of electrodes modified with FcC_6 (Fig. 2a) and FcC_{10} (Fig. 2c) is close to the maximum theoretical value (4.5×10^{-10} mol cm^{-2}) calculated for a close-packed monolayer of ferrocene derivatives.[19] However, electrodes modified by immersion in more concentrated solutions exhibit higher coverages (Table 1). The coverage ranged from 2 to 6 times the expected value for a monolayer and depended on the concentration of the solution. For the layers shown in Fig. 2 the coverages are equivalent to nearly 6 monolayers. The amount of compound deposited on the gold surface depends on the concentration of the deposition solution, temperature and light; however, the influence of the latter two was not systematically investigated in this work; hence, the modified electrodes reported here were formed in the dark at room temperature.

The layers were shown to be stable when subjected to repetitive cycling at different sweep rates. The film with the higher charge (FcC_6) was also placed in an ultrasonic bath for 2 min in an ethanol/water solution and only a very slight decrease in the charge under the ferrocene redox peaks was detected afterwards.

Half-wave potentials for the layers prepared from FcC_6 (Fig. 2a and 2b) are very close, suggesting that the same redox process is occurring. Identical behaviour is also observed for the FcC_{10} layers. However, the peak separation increases with increased charge (especially for layer 2d), which implies increased electrochemical pseudo-reversibility in the thicker layers. The major differences between the voltammograms of a monolayer and a layer with a high ferrocene coverage, are in terms of the $\Delta E_{p,1/2}$ values and the ratio i_p^{ox}/i_p^{red}. The oxidation peak becomes considerably sharper than the corresponding reduction peak, and the anodic peak current is much higher than the cathodic one. However, the charges consumed during the oxidation and reduction steps were equal.

For an ideal Nernstian reaction under Langmuir isotherm conditions, where the interactions between the electroactive adsorbates are minimal, a value of total width at half

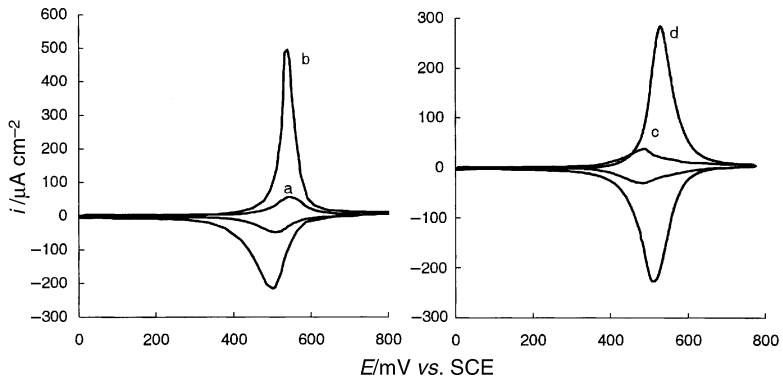

Fig. 2 Cyclic voltammograms of modified gold (111)-coated glass electrodes in 1 mM solution of FcC_6 (a) and FcC_{10} (c), and in 40 mM solution of FcC_6 (b) and FcC_{10} (d). The electrolyte solution was 1 M $HClO_4$ and the voltammograms were recorded at 100 mV s^{-1} starting from a potential of 0 V.

Table 1 Electrochemical data extracted from the voltammograms shown in Fig. 2

FcC_n	$E_{1/2}$ /mV ±5 mV	ΔE_p /mV ±5 mV	ΔE_{FWHM} /mV ± 5 mV ox.	red.	i_p^{ox}/i_p^{red}	$\Gamma/10^{-10}$ mol cm^{-2} ±0.2 × 10^{-10} mol cm^{-2}
FcC_6 (a)[22]	525	40	95	95	~1	3.8
FcC_6 (b)	520	45	35	90	2.3	24.2
FcC_{10} (c)[22]	490	0	100	100	~1	4.2
FcC_{10} (d)	510	30	65	90	1.3	21.7

maximum of 90.6/n mV (at 25 °C) can be expected.[20] Voltammograms of modified electrodes with a single layer (2a and 2c) of ferrocenyl alkyl thiols exhibit $\Delta E_{p,1/2}$ values very close to the theoretical one, which gives a qualitative indication of an ordered layer where the ferrocene centres share a similar environment within the monolayer, with minimal interactions between them. Sharper peaks and spikes have been observed for monolayers of similar compounds (prepared from concentrated thiol solutions),[21] electrodes coated with electroactive polymers[1] and in systems where no redox reactions occur.[21] The presence of sharp peaks is still unclear and has been attributed to many reasons including: (1) Formation of "phases" that may be poorly solvated, (2) structural change upon oxidation to ferricenium and (3) strong interactions between electroactive groups. It is worth noting that we detected sharp oxidation peaks only for electrodes with excess surface coverage of ferrocenyl alkyl thiols but never for monolayers. This may be an indication that for higher surface coverages the interaction between the electroactive groups increases. Furthermore, we anticipate that phase formation may be taking place, with the hydrophobic ferrocene groups being transformed to the more hydrophilic ferricenium moieties.

As is characteristic for an adsorbed redox centre, the peak currents (anodic and cathodic) for the monolayers 2a and 2c were found to increase linearly with the potential scan rate.[22] However, an unexpectedly different behaviour was observed for layers 2b and 2d. Fig. 3(a) shows plots of the anodic and cathodic current densities *vs.* sweep rate for the layer 2b (similar behaviour was observed for layer 2d). The non-linearity observed for the anodic process, points to the presence of a distinct mechanism during the oxidation of ferrocene, when the surface concentration is higher than a monolayer. However, the cathodic current density varies linearly with the sweep rate. Furthermore, linearity between the anodic peak current and the square root of sweep rate was observed for sweep rate values higher than 100 mV s^{-1} as is shown in Fig. 3(b). The difference between the oxidation and reduction steps was further confirmed by examining plots of ln I *vs.* ln v. For the reduction process, a slope of 0.92 was calculated whereas the oxidation step exhibited two slopes: 1.1 for sweep rates between 10 and 100 mV s^{-1} and 0.61 for sweep rates between 150 and 400 mV s^{-1}. This clearly indicates that the forward and reverse processes occur *via* different pathways. Many factors can contribute to this such as: the ohmic drop across the film and mixed control at higher sweep rates with mass transport occurring through diffusion/migration. It is also important to highlight that the ingress of ions and solvent during oxidation is similar to that observed in membranes and as such may be an activated process. It is not possible at this stage to pinpoint the exact mechanism. However, such hysteretic processes are not unknown in electrochemistry. Indeed many elaborate models exist in the literature to describe systems in which a catastrophic phase change occurs[23] which will lead to what has been described as systems with N-shaped Gibbs energy curves; that is systems that show spontaneous transitions at critical points.[24]

In conclusion, the discrepancy between the oxidation and reduction processes in what we shall term *multilayers* points to different environments of the redox centres in these two states. This could be related to the relative hydrophobicity of ferrocene and ferricenium, which can play an important role in these high coverage modified surfaces, together with ion pair formation between the ferricenium cation and the perchlorate anion.[25]

At this point the following question must be asked: How are the molecules assembled at the gold surface? A multilayer structure with physisorption interactions (similar to those observed in Langmuir–Blodgett films) between adjacent layers could be one possibility.[5,7] However, the stability shown by these modified electrodes, during the electrochemical cycling and when treated in an ultrasonic bath, seems to indicate stronger bonding between molecules.

It is known that hydrogen bonding is involved in stabilising SAMs. Boal and Rotello[26] examined the effect of *intra* and *inter* monolayer hydrogen bonding on the stability of amide-functionalised alkyl thiol SAMs on gold nanoparticles. The authors concluded that the position of the amide functionality was crucial to the extent of hydrogen bonding which was weakest when the amide group was close to the surface. However, when the amide group was separated from the surface by a long alkyl chain, an interdigitated structure was stabilised through hydrogen bonding, creating a large amorphous self-assembled nanoparticle ensemble. Clegg and Hutchison[27] also examined amide-containing alkyl thiol SAMs and concluded that hydrophobic interactions are of

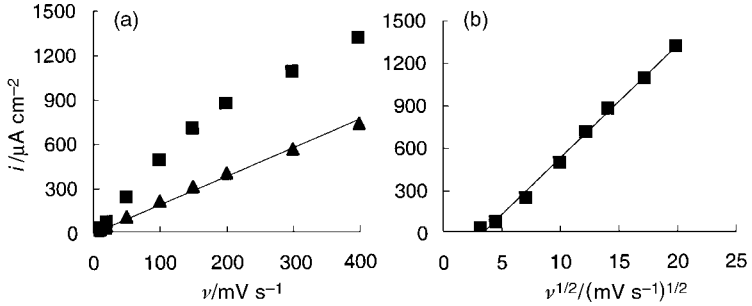

Fig. 3 Anodic (■) and cathodic (▲) peak current dependence on the scan-rate (a) and anodic (■) peak current dependence on the square root of the scan rate (b) recorded with the modified electrode of Fig. 2b.

secondary importance to hydrogen bonding in establishing film order and stability. Therefore, in the multilayers examined in this work, hydrogen bonding may be the cause of stabilisation of the structure. It is conceivable that the hydrogen of the SH group can be used to bridge one molecule to another through the carbonyl group, thus creating a ladder structure. In that case, only one monolayer is chemisorbed onto the gold surface with the other layers branching out.

In order to confirm this hypothesis and to compare the nature of the attachment of multi- and monolayers on the gold surface, reductive desorption studies were performed on two films assembled under different experimental conditions. Fig. 4 shows the voltammograms for (a) an FcC_{10} monolayer and (b) an FcC_6 multilayer in 0.5 M KOH. These films yield surface coverages of 5.2×10^{-10} (Fig. 2c) and 30.0×10^{-10} mol cm^{-2} (Fig. 2b) respectively based on the area under the redox peaks of the ferrocene.

The voltammograms in Fig. 4 were chosen for two reasons: to show the influence of the length of the alkyl chain and to compare the responses of multi- and monolayers. The position of the reductive peak for a monolayer depends on the length of the alkyl chain; longer chains yield more negative peak potentials.[1] However, the area of the peak ($\sim$90 μC cm^{-2} for alkyl thiols[1]) is independent of the length of the alkyl chain. The peak is assigned to the reductive desorption of the thiolate:

$$Au(I)SC_nX + e^- + M^+ \rightarrow Au(0) + XC_nS^-M^+ \qquad (1)$$

The stripping peak potentials obtained from the voltammograms (Fig. 4) are −1015 mV for FcC10 monolayer and −990 mV for the FcC6 film, which is in good agreement with the previously observed behaviour for monolayers of different alkyl chain length. The more surprising result was that the charges involved in the reductive stripping processes for the monolayer (96 μC cm^{-2}) and the multilayer (98 μC cm^{-2}) were nearly the same. Eqn. (1) implies that only one electron is transferred during the desorption process which when taking the roughness factor into account, indicates the stripping of approximately one monolayer from each electrode.

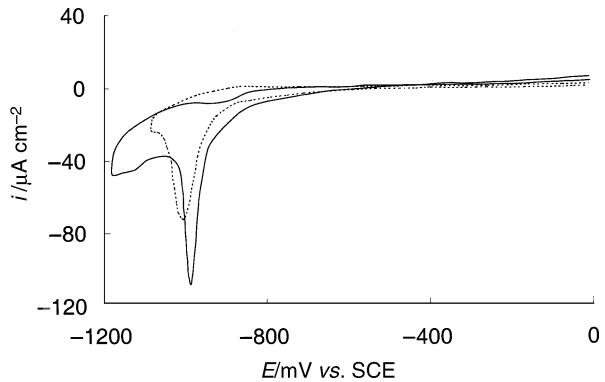

Fig. 4 Cyclic voltammograms of modified gold with 3 mM solution of FcC_{10} (a, ····) and 40 mM solution of FcC_6) (b, →) in 0.5 M KOH. The sweep rate was 50 mV s^{-1} starting from a potential of 0 V.

This means that the amount of thiolate chemically bonded to the gold electrode, for a multilayer with 30×10^{-10} mol cm^{-2} of ferrocene derivative coverage is the same as that obtained for a monolayer formed from similar compound. This clearly confirms that all the material in the multilayer cannot be chemically adsorbed to the Au surface. Using an electrochemical quartz crystal microbalance (EQCM) Schneider and Buttry[7] reported the presence of excess alkyl thiols (without any electroactive groups) at Au(111) and suggested that the majority of the compound is physically adsorbed onto the partially formed underlying monolayer of chemisorbed material. However, the excess alkyl thiol was reported to slowly evolve into a monolayer with prolonged adsorption time. Our results point to a much more stable, multilayered structure which evolves with deposition time. One experimental method that can provide evidence for the existence of multilayers is ellipsometry.

Ellipsometric studies

Ellipsometry is a very sensitive optical technique, which is particularly useful for the *ex situ* or *in situ* characterisation of thin layers on surfaces.

Values for the complex refractive index ($\hat{n} = n - ik$, where n is the refractive index and k the absorption index) and the average thickness of the layers were estimated using the three-phase model, from the change in the ellipsometric parameters between the bare and modified gold surfaces. The three-phase model consists of substrate/layer/ambient medium. Since the layers were not transparent (k small but not zero), the evaluation of the optical constants and thickness, from $\delta\Psi$ and $\delta\Delta$, was not straightforward. One of the unknowns had to be reasonably introduced to deduce the other two. First, assuming n as 1.45, which is the value estimated for the refractive index of alkyl thiols,[21] k and the thickness values were calculated. Secondly, the dimensions of the compound were predicted based on estimated values, and a series of thicknesses close to that value were introduced to evaluate n and k. The average thickness values for the modified electrodes from dilute solutions of ferrocene alkyl thiols of different chain lengths are summarised in Table 2. Based on previous ellipsometric studies (20 Å for $CH_3(CH_2)_{10}SH$; 1.1 Å per CH_2 and 7 Å for the ferrocene group[28]), the expected value for a FcC_6 monolayer is about 23 Å. The data obtained for films prepared from dilute solutions are within the expected range for a monolayer; for example the thickness calculated for an FcC_6 monolayer was 25 Å. However, these values, as well as the majority of the published data, are higher than the values calculated from molecular dimensions (19.1 Å for FcC_6). This discrepancy has been attributed to the chemisorption of thiol to form thiolate that must produce a change in the electron density at the gold surface, especially for ultrathin molecular layers. Even with these limitations, the thickness values for the monolayers examined here show very clearly the influence of increasing the length of alkyl chain and indeed confirm the sensitivity of the method.

The estimated thickness values for the multilayers (Table 2) are much higher than those obtained for monolayers, which is

Table 2 Thickness values determined from ellipsometry and surface coverages calculated from voltammetry for gold-coated glass electrodes (111) modified in dilute (1–3 mM) and concentrated solutions (30 to 40 mM) of FcC_n

	Dilute solution		Concentrated solution	
Compound	Thickness/Å	$\Gamma/10^{-10}$ mol cm^{-2}	Thickness/Å	$\Gamma/10^{-10}$ mol cm^{-2}
FcC_3	21 ± 2	3.2	142 ± 12	12.0
FcC_4	23 ± 2	3.3	67 ± 4	6.4
FcC_6	25 ± 2	3.8	210 ± 20	18.8
FcC_{10}	29 ± 3	4.2	88 ± 6	8.8

in agreement with data obtained from the electrochemical studies in that monolayers or multilayers are formed depending on the deposition conditions.

A two-layer model was further applied to check if the optical parameters of the first layer are different from the subsequent layers. The data indicate the presence of layers with the same optical properties which also confirms the conclusions drawn from the electrochemical measurements that indicate that the nature of the layers does not change with the thickness ($E_{1/2}$ values were similar for mono and multilayers).

Imaging ellipsometry was then used for the characterisation of the layers previously measured by conventional ellipsometry. This recent technique enables the visualisation of the lateral thickness distribution of a layer deposited on a substrate. This method is very sensitive for detecting small thickness variations (better than 0.5 Å) in thin films.

Fig. 5 shows images of organised mono and multilayers of FcC_6 assembled under different conditions. The resulting images are in agreement with conventional ellipsometry and electrochemical methods in that they enable the visualisation of mono- or multilayers formed as a function of the deposition conditions. Fig. 5(a) shows an image of a homogeneous film of a monolayer evolving from the bare substrate; this monolayer is the same as that used to calculate the 25 Å thick monolayer in Table 2. The soft transition from the bare gold substrate to the monolayer is likely to be due to the adsorption of material at the meniscus and the mobility of the gold thiolate; the latter will be discussed in the SPM section. Therefore, the amount of adsorbate per cm^{-2} present at the edges of the monolayer will be less than in the monolayer, hence the orientation of the molecules may not be perpendicular or near perpendicular, resulting in a what looks like a thinner film.

When part of the monolayer was further immersed in a more concentrated solution of the thiol (30 mmol dm^{-3}), a thicker structure evolves (210 Å) from the monolayer as shown in Fig. 5(b). Imaging ellipsometry was particularly useful in confirming the presence of layers with different thicknesses depending on the layer preparation.

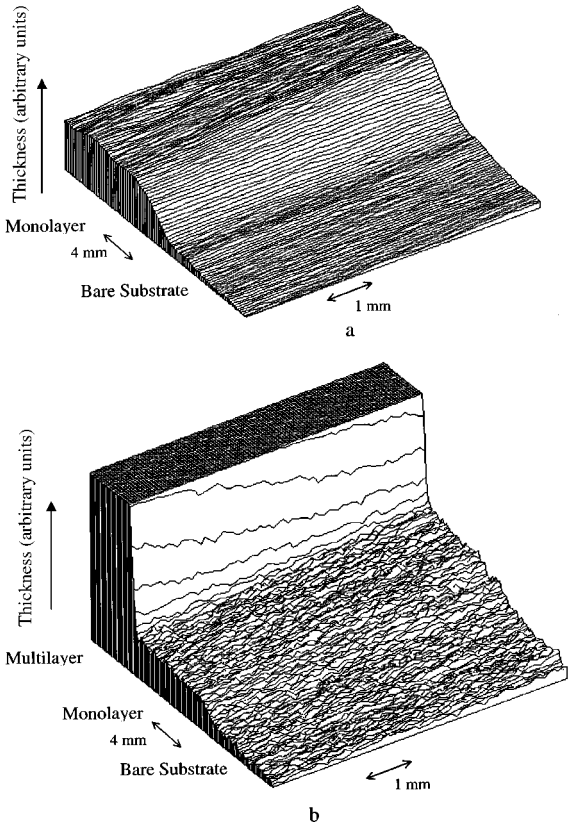

Fig. 5 Thickness distribution for two samples of FcC_6 on Au(111)-coated glass slides obtained from imaging ellipsometry. (a) Half a slide was immersed in 3 mM of thiol solution for 20 h; (b) 2/3 of the slide were immersed in 3 mM solution for 4 h followed by 1/3 immersion in 30 mM solution for 20 h. The flat region in the image (5b) corresponds to equipment saturation which was allowed to occur to enable the monitoring of the monolayer in the same image.

Scanning probe microscopy of Fe thiol modified surfaces

Scanning probe microscopy has been used to examine the surfaces of gold modified electrodes formed from both dilute and concentrated solutions of FcC_6. Fig. 6 shows an STM image of a flame annealed gold coated glass sample before modification. The roughness level is low, with a measured RMS roughness of $R_q = 0.131$ nm. The typical well-defined step and terrace morphology is apparent. The 60° and 120° intersecting step edges point to a (111) surface morphology, which has been resolved at atomic resolution in separate experiments.

Clean gold surfaces, in the absence of adsorbates show rather limited mobility. However, remarkable mobility can be induced in the presence of adsorbates such as chloride ions.[29]

Following treatment with dilute solutions (2.5 mmol dm^{-3} with an immersion time of approximately 30 min) the surface still exhibits single atomic height step and terrace morphology, as shown in Fig. 7. It is apparent, however, that the step morphology no longer shows the characteristic 60° and 120° intersecting straight step edges. The steps are clearly modified after exposure to the dilute FcC_6 solutions. Images taken over a period of several minutes show step etching of a type that has previously been observed for gold surfaces in contact with

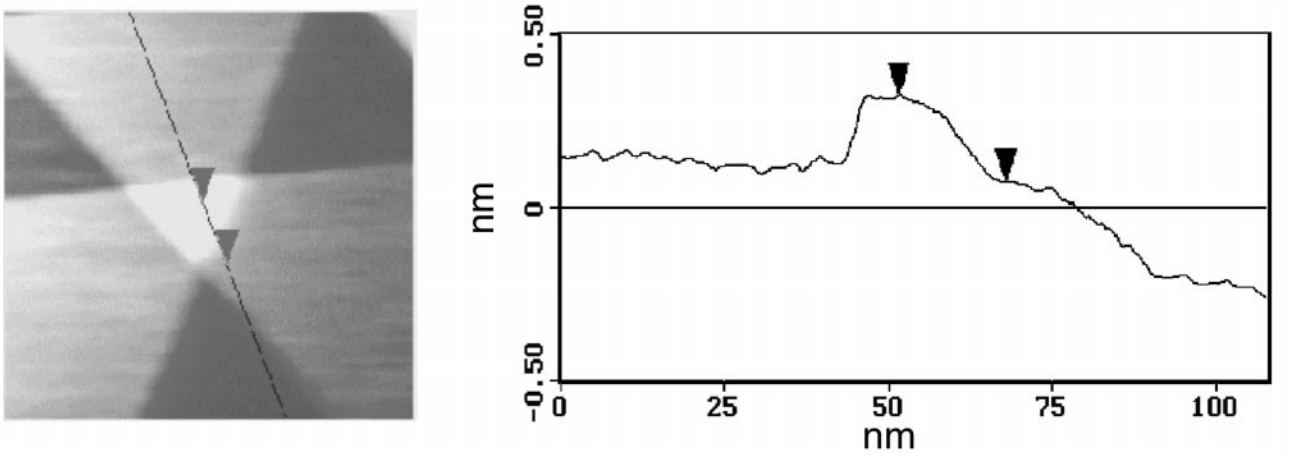

Fig. 6 An STM image (100 nm × 100 nm) of a flame annealed gold on glass substrate surface showing typical Au(111) morphology. A cross-section through the image is also included.

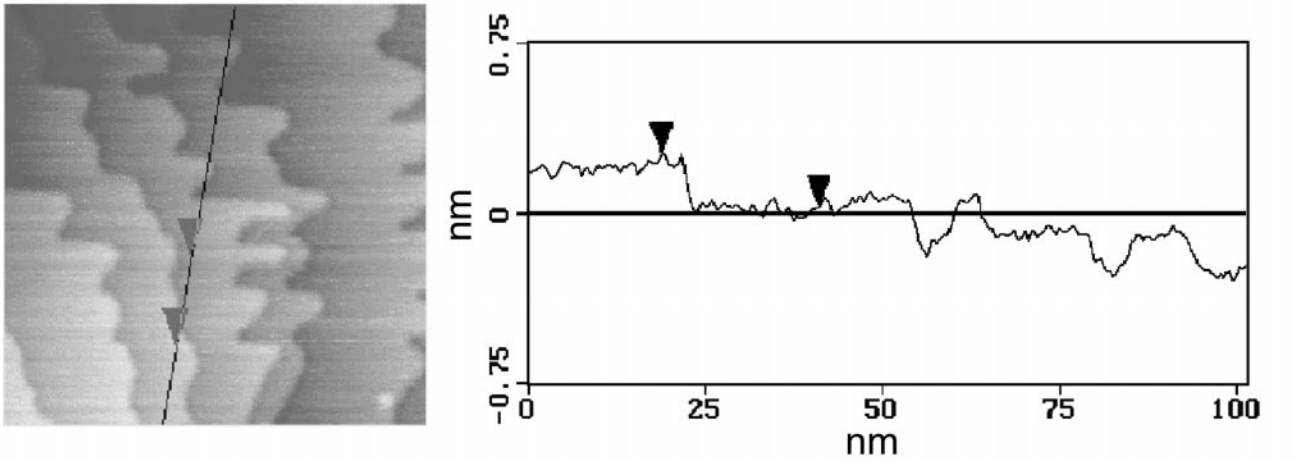

Fig. 7 An STM image (100 nm × 100 nm) and the corresponding cross-section of a gold on glass substrate after exposure to low concentration FcC_6 solution (2.4 mmol dm^{-3}) with an immersion time of approximately 30 min.

tetramethylthiourea (TMTU) containing electrolytes.[30] As for TMTU covered Au(111) electrode surfaces, the FcC_6 adsorbate promotes surface mobility and the etching of gold steps. This behaviour indicates that the strong Au–sulfur bond mediates the detachment of gold atoms from step edges. The work described here is mainly focussed on the formation of multilayers, hence the issue of etching and surface mobility will be addressed in greater detail in a separate publication.

Although step etching was observed, no pitting of terraces was apparent, indicating that the more highly co-ordinated terrace atoms can resist at least the lower concentrations of FcC_6 solution. Although atomic resolution of the Au(111) surface atoms could be obtained on unmodified surfaces, no molecular resolution of the FcC_6 could be observed for the modified surfaces. It is likely that this inability to resolve the FcC_6 adsorbate at molecular level arises from the mobility of the surface layer as apparent from the step edge mobility. There may also be mobility or disorder in the alkyl chains of the adsorbate, which prevents a high-resolution imaging. The modified surface exhibited a level of roughness greater than that observed for the bare surface, with a measured RMS roughness of $R_q = 0.22$ nm.

The resolution of step and terrace features after exposure of the surface to dilute solutions of FcC_6 is consistent with ellipsometric measurements of film thickness under similar conditions. The ellipsometry data show film thickness that varies from 2.1–2.9 nm for FcC_3 to FcC_{10}, which is consistent with monolayer coverage. It is unlikely that substrate features such as monatomic step edges would be observed for film thickness much greater than about a monolayer. Therefore the STM images are consistent with coverage not exceeding about a monolayer. Indeed, the following paragraph shows that the morphology following exposure to high concentrations of FcC_6 is substantially different.

Fig. 8 shows a tapping mode AFM image of an Au(111) surface that had been immersed in 25 mM FcC_6 in toluene for 24 h. Stable STM images could not be obtained for such surfaces, probably because of difficulty in obtaining a stable tunnelling current response through the thicker FcC_6 films. Tapping mode AFM is a non-destructive technique, which probes ("taps") the surface without permanent contact and it is particularly useful for imaging soft, rough or "sticky" surfaces. For instance, this method has been used to image activated polyimide surfaces, which show a high tip-to-sample adhesion during contact mode imaging.[31]

Fig. 8 is a typical tapping mode image of the FcC_6 covered surface resulting from exposure to concentrated solutions. It is clear from the peak to peak roughness (3.36 nm) of the surface that this image no longer represents monolayer covered Au(111) substrates. Indeed, these images are consistent with multilayer coverage. This is clearly consistent with the ellipsometric data in Table 2, which shows for instance, a thickness of 14.2 nm for FcC_3 and a thickness of 6.7 nm for FcC_4 exposure at high concentration. As expected the overall

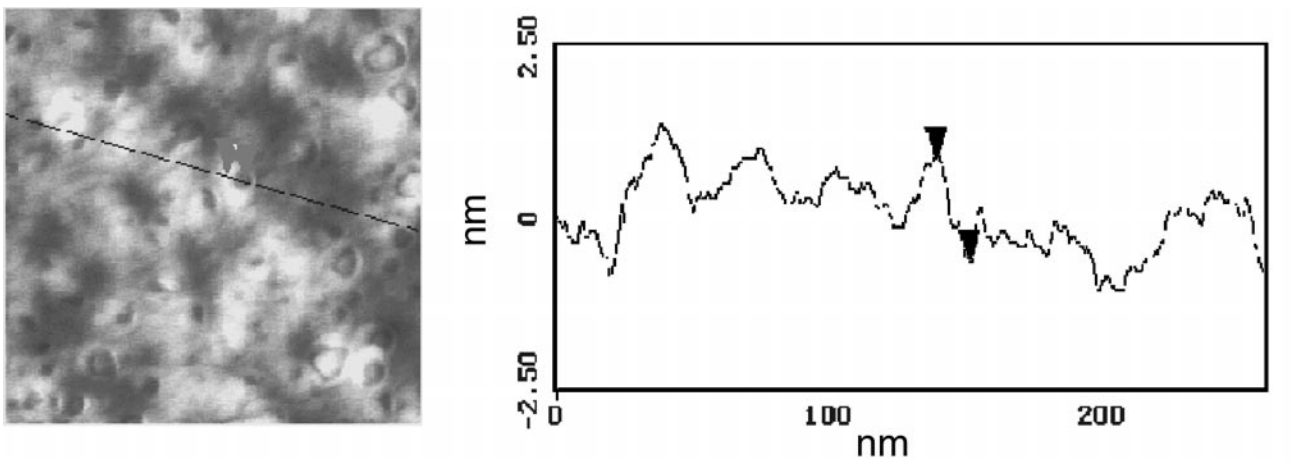

Fig. 8 A tapping mode AFM image (200 nm × 200 nm) with the corresponding cross-section of a gold on glass substrate after exposure to a high concentration (25 mM) FcC_6 solution in toluene for 24 h.

roughness of the modified surface following an extended immersion period at high FcC_6 concentrations increases giving a measured RMS roughness of $R_q = 0.462$ nm.

The tapping mode AFM data also reveal a characteristic structure for the multilayer-covered surface. This surface can be described as consisting of grains or nodules as well as annular structures which penetrate into the surface. Cross-sectional plots show that the individual nodules exhibit a diameter distribution of between 20 to 50 nm. There is also a high density of annular shaped features, which have a diameter range of 10 to 20 nm. The diameter of the annular-shaped features measured consistently at 15 ± 2 nm.

In summary, electrochemical, ellipsometric and SPM data highlighted the importance of the concentration of the deposition solution and confirmed that solutions with higher concentration of thiols resulted in multilayered structures.

Spectroscopic studies

Electrodes modified with multilayers were also characterised using *in situ* FTIR spectroscopy in order to try and elucidate any differences, at the molecular level, that may exist between mono and multilayers.

We have previously shown[22] that monolayers of the same thiols examined in this work undergo a redox-induced reorientation due to the formation of the ferricenium cation. This orientation was manifested by the rotation of the ferrocene rings. We assigned the differences in the IR response of the several monolayers studied to a distinct orientation of the molecules attached to the electrode surface.

Fig. 9 shows two difference spectra obtained at 600 mV (normalised against the spectra collected at 200 mV) for (a) a FcC_6 monolayer and (b) a multilayer ($\Gamma = 2 \times 10^{-9}$ mol cm^{-2}) in 0.5 mol dm^{-3} $HClO_4/D_2O$. From Fig. 9 and Table 3, it is possible to observe that the main peaks obtained for the multilayer, after the oxidation of the ferrocene, are the same as the ones for a monolayer. However, the integrated areas of the IR bands corresponding to the multilayer are much higher. Therefore, the spectroscopic data also confirm the presence of larger quantities of the ferrocene derivative at the surface than is expected for a monolayer.

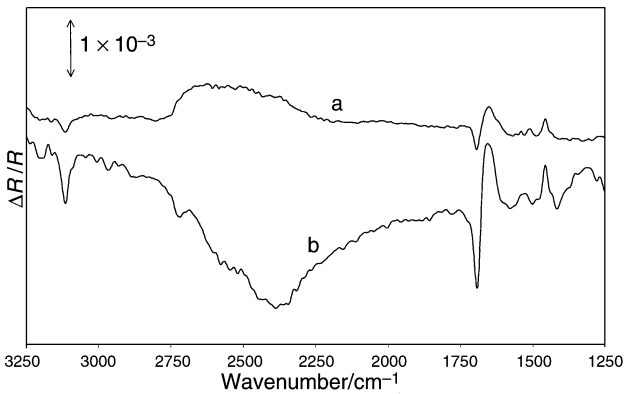

Fig. 9 SNIFTIRS spectra of two gold modified electrodes in (a) 3 mM and (b) 40 mM solution of FcC_6. The spectra were obtained at 600 mV (using as reference the spectra at 200 mV) in 0.5 M $HClO_4/D_2O$.

Table 3 Vibrational modes obtained from the SNIFTIR spectra $[(E_{600} - E_{200})/E_{200}]$ of a layer prepared from immersion of a single-crystal Au(111) disc in a 40 mM solution of FcC_6

Vibration mode	Wavenumber/cm^{-1}
ν(C–H)	3113↓
ν(C=O) Fc^+	1693↓
ν(C=O) Fc	1663 and 1655↑
ν(Fc–C=O) + $\delta(CH_2)$	1454↑
Fc^+ ring mode	1419↓

However, there are two major differences between the SNIFTIR spectra of the mono- and multilayer. Firstly, there is a large absorption in the spectrum of the multilayer, centred on 2400 cm^{-1}. This is associated with the influx of D_2O accompanying the ingress of the anions into the film. Similar behaviour has been observed for conducting polymer films on surfaces. This is not expected to occur in monolayers as the redox active centre is at the end of the chain in contact with electrolyte, thus eliminating the need for the insertion of hydrated anions.

The second and more interesting observation is related to the appearance, in multilayers, of a downward pointing band at 2670 cm^{-1}. This band may be associated with the S–H bond. The sign of the band indicates that its population increases with increased positive potential. This band also appears in the spectra of multilayers of FcC_5, FcC_6 and FcC_{10} as shown in Fig. 10 and its intensity increases with increasing chain length.

It is worth recalling here the findings of Boal and Rotello[26] in which it was concluded that H-bonding becomes important as the distance of the centre taking part in that bonding is moved away from the surface. This band is not observed in FcC_3 but its intensity increases as the chain length increases. It is not unreasonable to assume that the hydrogen of the thiol group in the second layer can form a hydrogen bond with the carbonyl group of the first monolayer. However, after oxidation, the ferricenium centre can act as a Lewis acid which is capable of binding to the sulfur of the molecule in the adjacent layer through a dative bond which will eventually weaken the extent of hydrogen bonding and effectively "free" the SH from that bond. Thus the SH bond appears as the potential is made more positive.

Based on these findings, we conclude that hydrogen bonding is responsible for maintaining the multilayered structures reported in this work.

However, it is worth pointing out that even though the multilayers were stable when the potential was continuously cycled, a loss in electroactivity (37%) was noted when the potential was held at potentials more positive than 600 mV for prolonged periods. However, this loss in activity occurred only when the film was reduced. SNIFTIR spectra recorded at 600 mV for varying periods showed no loss when the potential was kept at that value, however, a loss in the ν(C=O) absorb-

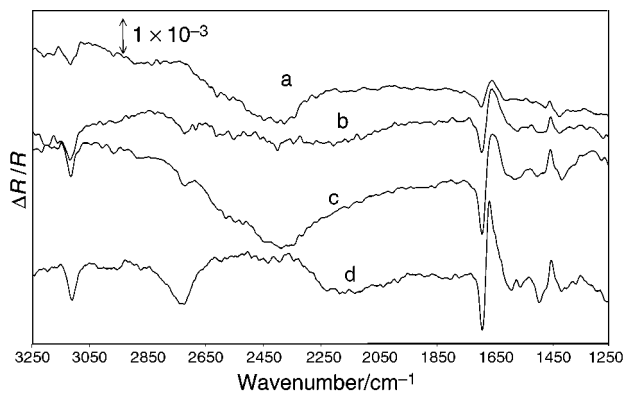

Fig. 10 SNIFTIR spectra for a single-crystal gold (111) disc modified with concentrated solutions (30–40 mM) of (a) FcC_3, (b) FcC_5, (c) FcC_6 and (d) FcC_{10} in 0.5 M $HClO_4$ and D_2O, where the average surface coverage was 2×10^{-9} mol cm^{-2}. The spectra were obtained at 600 mV and normalised against the spectra recorded at 200 mV.

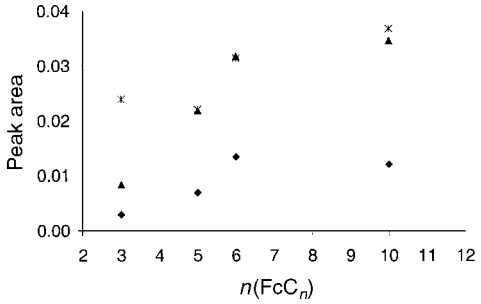

Fig. 11 Peak area dependence on the alkyl chain length for three major bands assigned in Table 2: 3200 (*), 1693 (▲) and 1454 cm^{-1} (◆).

ance (35%) was observed when the potential was stepped back to 0 mV and back again to 600 mV. We are unsure yet as to the origin of this observation.

The effect of the length of the alkyl chain in the monolayer orientation with the potential was also examined. The spectra shown in Fig. 9 were obtained from multilayers with $\Gamma = 2 \times 10^{-9}$ mol cm^{-2}. Although the same general behaviour is observed for the different compounds, the intensities of the bands seem to be dependent on the length of the alkyl chain. The effect of the chain length on the peak areas of three of the major bands assigned in Table 3 is illustrated in Fig. 11. The data point to a trend towards higher peak areas as the length of the alkyl chain increases, reaching a plateau at FcC_6 layer. It is quite surprising that even though the quantities of materials are the same in each case, the intensities decrease with decreasing chain length.

The reason for this behaviour may be attributed to the degree of order in the multilayers. The surface selection rules indicate that p-polarised radiation interacts with vibrations that have a vector of the dipole moment perpendicular to the surface. Thus we conclude that multilayers of longer alkyl chains are more ordered. The shorter chains are disordered and a large fraction of the molecules are not aligned perpendicular to the surface. The fact that shorter chains result in disordered films is well known in the field of self-assembly.

Analysis of the SNIFTIR spectra of the monolayers[22] showed that the band around 1660 cm^{-1} (ν(C=O)) is broader than the negative going band. This behaviour suggested that for shorter-chain compounds the ferrocene moieties share different environments in the layer. However, the same peaks for the longer compound studied were sharper and more symmetric, which indicates that the layers of the latter are more ordered.

Conclusions

Using a variety of electrochemical, spectroscopic and scanning probe microscopic methods, we showed that under certain conditions, self-assembled multilayers could be formed instead of self-assembled monolayers. The thickness of the multilayers can be controlled by varying the concentration of the deposition solution. Analysis of the voltammetric response of the mono- and multilayers in addition to SNIFTIR spectra indicated that the oxidation of multilayers follows a mechanism distinctly different to the reduction step, whereas, as expected, the redox switching of the monolayers is kinetically controlled.

STM, AFM and ellipsometry confirmed the presence of multilayers, whose thickness values were in agreement with those calculated from the redox charge. It is likely that hydrogen bonding is responsible for maintaining the structural integrity of the multilayers.

Acknowledgements

The authors (AV, LMA and MK) would like to acknowledge the financial support from Fundação para a Ciência e Tecnologia, grant number PRAXIS XXI BD/11044/97, and the EPSRC (UK). The authors would also like to thank Dr Ian Butler for his assistance with the chemistry of ferrocene and Mr David Ellis for synthesising the compounds.

References

1 H. O. Finklea, in *Electroanalytical Chemistry: A Series of Advances*, ed. A. J. Bard and I. Rubinstein, Marcell Dekker, New York, 1996, vol. 19.
2 S. Arnold, Z. Q. Feng, T. Kakiuchi, W. Knoll and K. Nikki, *J. Electroanal. Chem.*, 1997, **438**, 91.
3 G. Che, Z. Li, H. Zhang and C. R. Cabrera, *J. Electroanal. Chem.*, 1998, **453**, 9.
4 T. Kondo, M. Takechi, Y. Sato and K. Uosaki, *J. Electroanal. Chem.*, 1995, **381**, 203.
5 R. C. Thomas, L. Sun, R. M. Crooks and A. J. Ricco, *Langmuir*, 1991, **7**, 620.
6 Y. Kim, R. L. McCarley and A. J. Bard, *Langmuir*, 1993, **9**, 1941.
7 T. W. Schneider and D. A. Buttry, *J. Am. Chem. Soc.*, 1993, **115**, 12391.
8 C. C. Bamdad, G. B. Sigal, J. L. Stominger and G. M. Whiteside, *US Pat.*, 5 620 850, 1997.
9 P. Ruger, D. Ambrosius, B. Schmidt, P. Sluka, H. Guder and E. Kopetzki, *US Pat.*, 5 834 224, 1998.
10 I. Yuichi and M. Akira, *Jpn. Pat.*, JP6003316A2, 1994.
11 S. Creager and K. Olsen, *Anal. Chim. Acta*, 1995, **307**, 277.
12 H. Lee, L. J. Kepley, H.-G. Hong and T. E. Mallouk, *J. Am. Chem. Soc.*, 1988, **110**, 618.
13 K. Weber, L. A. Hocket and S. E. Creager, *J. Phys. Chem.*, 1997, **101**, 8286.
14 G. K. Rowe and S. E. Creager, *Langmuir*, 1994, **10**, 1186.
15 M. S. Ravenscroft and H. O. Finklea, *J. Phys. Chem.*, 1994, **98**, 3843.
16 A. Jones, PhD Thesis, University of Wales, Bangor, 2001.
17 W. Haiss, D. Lackey, J. K. Sass and K. H. Besocke, *J. Chem. Phys.*, 1991, **95**, 2193.
18 G. Jin, P. Tenvall, I. Lundström and H. Arwin, *Anal. Biochem.*, 1995, **232**, 69.
19 C. E. D. Chidsey, C. R. Bertozzi, T. M. Putvinsky and A. M. Mujsce, *J. Am. Chem. Soc.*, 1990, **112**, 4301.
20 A. J. Bard and L. Faulkner, *Electrochemical Methods: Fundamentals and Applications*, Wiley, New York, 1980.
21 K. Uosaki, Y. Sato and H. Kita, *Langmuir*, 1991, **7**, 1510.
22 A. S. Viana, A. Jones, L. M. Abrantes and M. Kalaji, *J. Electroanal. Chem.*, 2001, **500**, 290.
23 M. Kalaji, L. M. Peter, L. M. Abrantes and J. Mesquita, *J. Electroanal. Chem.*, 1989, **274**, 289.
24 S. Feldberg and I. Rubenstein, *J. Electroanal. Chem.*, 1988, **240**, 1.
25 D. Popenoe, R. S. Deinhammer and M. D. Porter, *Langmuir*, 1992, **8**, 2521.
26 A. Boal and V. Rotello, *Langmuir*, 2000, **16**, 9527.
27 R. S. Clegg and J. E. Hutchison, *J. Am. Chem. Soc.*, 1999, **121**, 5319.
28 T. Ohtsuka, Y. Sato and K. Uosaki, *Langmuir*, 1994, **10**, 3658.
29 D. J. Trevor, C. E. D. Chidsey and D. N. Loiacono, *Phys. Rev. Lett.*, 1989, **62**, 929.
30 E. Bunge, H. Meyer, H. Baumgaertel, B. Roelfs and R. J. Nichol, *Langmuir*, 1996, **12**, 3060.
31 D. Schröer, PhD Thesis, The University of Münster, Germany, 1994.